© 2020. Published by The Company of Biologists Ltd | Development (2020) 147, dev183277. doi:10.1242/dev.183277

RESEARCH ARTICLE

Spatiotemporal control of cell growth by CUC3 shapes leaf margins

Léo Serra*,‡ and Catherine Perrot-Rechenmann‡

ABSTRACT

How a shape arises from the coordinated behavior of cells is one of the most fascinating questions in developmental biology. In plants, fine spatial and temporal controls of cell proliferation and cell expansion sustain differential growth that defines organ shape and size. At the leaf margin of *Arabidopsis thaliana*, interplay between auxin transport and transcription factors named CUP SHAPED COTYLEDON (CUCs), which are involved in the establishment of boundary domain identity, were reported to trigger differential growth, leading to serration. Cellular behaviors behind these differential growths remain scarcely described. Here, we used 3D and time lapse imaging on young leaves at different stages of development to determine the sequence of cellular events resulting in leaf serrations. In addition, we showed that the transcription factor CUC3 is a negative regulator of cell growth and that its expression dynamics in a small number of cells at the leaf margin is tightly associated with the control of differential growth.

KEY WORDS: *Arabidopsis thaliana*, Cell growth, Leaf development, Morphogenesis, 4D imaging, MorphoGraphX

INTRODUCTION

During their initial development, plant cells undergo mainly two types of processes: cell proliferation, which combines cell division per se (the partitioning of one cell into two daughter cells) and cell growth (increase in cell volume that occurs within the cell cycle); and cell expansion, which consists in an irreversible increase in the size of cells that have exited cell proliferation and is often associated with differentiation processes (Fleming, 2018; Perrot-Rechenmann, 2010). This increase in size varies in strong proportions according to the cell type and environmental cues. To date, it is not clear whether cell growth occurring within the cell cycle and later on cell expansion result from similar processes or not (Sablowski, 2016). At tissue or organ levels, growth results from the combination of proliferation and expansion; in shoots, spatial and temporal regulations of growth sustain the iterative formation of new growth axis (leaves, lateral branches and flowers), which is the basis for shoot architecture. Leaf morphogenesis is sustained by the iterative initiation of the new growth axis associated with serrations, lobes or leaflet formation, depending on the species.

Institut Jean-Pierre Bourgin, INRA, AgroParisTech, CNRS, Université Paris-Saclay, 78000, Versailles, France.
*Present address: The Sainsbury Laboratory, University of Cambridge, Cambridge CB2 1LR, UK.

‡Authors for correspondence (leo.serra@slcu.cam.ac.uk; catherine.rechenmann@cnrs-dir.fr)

L.S., 0000-0001-5564-7299; C.P.-R., 0000-0002-7355-0121

Received 30 July 2019; Accepted 14 February 2020

In land plants, initiation of new growth axis generally relies on the competency of cells to divide and the maintenance of founder cells with an undifferentiated cell fate. Although the undifferentiated state of shoot apical meristem (SAM) cells is conserved across species, the spatial and temporal regulation of proliferation in leaves differs between species. In general a longer proliferation phase is associated with a higher number of initiated leaf marginal outgrowths, e.g. tomato and *Cardamine hirsuta* leaves exhibit a longer proliferation phase in comparison with *Arabidopsis* and initiate a higher number of marginal outgrowths. Important regulators of the undifferentiated fate are the KNOX family of transcription factors (TFs), such as SHOOTMERISTEMLESS, which shows conserved expression in the SAM across species, whereas its expression varies in leaves of distinct species in correlation with the number of marginal outgrowths (Hay et al., 2002; Kierzkowski et al., 2019; Piazza et al., 2010).

Another feature required for initiation and maintenance of new growth axis is the spatial organization of growth. High-growing regions, such as primordia in the peripheral zone of the SAM and leaf marginal outgrowth, are spatially isolated from surrounding regions by a domain of lower growth: the boundary domain (Dumais and Kwiatkowska, 2002; Kwiatkowska, 2004). Beside the SAM and sinuses or inter-leaflet regions in leaves, boundary domains are found in numerous domains separating plant organs (Aida and Tasaka, 2006). Genetic approaches have shown that boundary domain formation requires the activity of CUC transcription factors. Disruption of CUC genes results in more or less severe defects in organ separation, depending on the gene and the species (Aida et al., 1997, 1999; Gonçalves et al., 2015; Vroemen et al., 2003). In leaves, regardless of the species, CUC loss of function always results in a simplification of leaf dissection (Berger et al., 2009; Blein et al., 2008); in *Arabidopsis thaliana*, *CUC1* ectopic expression or *CUC2* overexpression results in increased serrations or even formation of leaflets (Hasson et al., 2011; Takada et al., 2001). The formation of a new growth axis is associated with the establishment of auxin maxima mediated by dynamic polar auxin transport (Bilsborough et al., 2011; Kawamura et al., 2010; Reinhardt et al., 2000, 2003). In leaf, it has been proposed that sequential formation of auxin maxima at the leaf margin was the result of interplay between the CUC2 and PIN1 polar auxin transporter, leading to auxin accumulation at the teeth and auxin depletion from the boundaries. In addition, auxin responses would restrict *CUC2* expression to the sinuses, thus forming a CUC2-PIN1-Auxin module enabling the reiterative formation of growth axis at the leaf margin (Bilsborough et al., 2011; Kierzkowski et al., 2019). This module is also involved in primordia initiation at the SAM periphery and during ovule primordia formation (Galbiati et al., 2013; Heisler et al., 2005; Vernoux et al., 2000). The recent technical advances in time-lapse imaging and image analyses allowed the identification of a strong correlation between regions of transcriptional auxin responses and CUC2 domains, and regions of high and low overall growth at the leaf margin of

Development (2020) 147, dev183277. doi:10.1242/dev.183277

A. thaliana, respectively (Kierzkowski et al., 2019). In addition to this module, the local expression of *REDUCED COMPLEXITY* (*RCO*), a TF that is absent in *A. thaliana*, in inter-leaflet regions of *C. hirsuta* leaves has been associated with regions of lower growth and division (Kierzkowski et al., 2019; Vlad et al., 2014).

In *A. thaliana* simple leaf, apart from CUC2, *CUC3* is the only other CUC gene being expressed, although with a slightly different pattern. CUC2 is localized in a broad domain at the leaf margin with a maximum in the region of sinuses, whereas *CUC3* is expressed in only a few cells at the sinuses (Maugarny-Cales et al., 2019). While *cuc2-1* loss of function exhibits a smooth margin as it fails to initiate teeth, the *cuc3-105* null mutant still initiates serrations but they tend to be rapidly smoothed during leaf development. In *A. thaliana* leaves, the effect of CUC2 on the maintenance of marginal outgrowth has been shown to partially rely on CUC3, as over-dissected leaves of *A. thaliana* lines exhibiting higher levels of CUC2 become smoothed in a *cuc3-105* mutant background (Hasson et al., 2011; Maugarny-Cales et al., 2019). Altogether, these results suggest distinct roles for CUC2 and CUC3, with the CUC2-PIN1-Auxin module required to sequentially initiate outgrowth at the leaf margin and CUC3 required for maintaining the growth of these new axes through a yet unknown mechanism.

Here, using a combination of 3D imaging and time-lapse experiments on leaf primordia of *A. thaliana*, we analyzed cellular behaviors at the abaxial epidermis and leaf margin during early stages of leaf development. We revealed that spatial and temporal regulation of cell growth mediated by CUC3 is required to modulate differential growth at the leaf margin, thus sustaining the dynamic changes of leaf shape over development.

RESULTS

Spatial differences in cell growth sustain differential growth at the leaf margin

In order to investigate the longstanding issue of cellular events occurring behind differential growth at the leaf margin, we used 3D imaging and time lapse experiments on lines expressing *p70::PIP2-GFP*, a plasma membrane marker (Luu et al., 2012) (Fig. 1A), to analyze cell behavior during early stages of teeth formation. We focused on the first teeth (referred to as teeth 1), which are the first ones to be formed on each margin of very young leaves of about 200 µm in blade length (Biot et al., 2016). Cell segmentation and growth analyses were performed using MorphoGraphX software (Barbier de Reuille et al., 2015) complemented by homemade pipelines that aimed to identify and analyze cellular or clonal parameters (see Fig. S1 for the image analyses pipeline). For each experiment, the first step was to determine, in a reproducible manner, cells of the abaxial epidermis belonging to sinus and tooth, respectively. To do so, we took advantage of geometric features of the leaf margin. Teeth are dome-shaped, whereas sinuses are saddle shaped; they thus exhibit positive and negative gaussian curvature, respectively. Once sinuses belonging to cells have been identified by threshold on the mean gaussian curvature of the leaf surface (measured per cell), we then defined the teeth as the region of epidermis between two successive sinuses on the margin side. For time-lapse experiments, we identified these two cell populations at the beginning of the experiment (time zero) to further define sinuses and teeth-derived clones (group of sister cells derived from a single mother cell at time 0) at 24 and 48 h (Fig. 1B). We then performed quantitative measurements of surface areas, and division and growth on these two types of clones (Fig. 1). As anticipated, differences in clone surface areas increase between sinus and tooth during tooth outgrowth, with sinus-derived clones being smaller than the tooth-derived clones (Fig. 1C,F). To determine whether this difference results from variations in division and/or cell growth, we analyzed the number of cells formed per clone from time zero to 48 h and computed the clone areal strain, defined as: [(clone surface area $_{\text{at 48h}}$−clone surface area $_{\text{at 0h}}$)/clone surface area $_{\text{at 0h}}$]×100 over the same time frame. During the early stages of tooth growth (40 µm to 100 µm in tooth width), the number of cell division events was not significantly different in the sinus in comparison with the tooth, indicating that spatial differences in number of cell division events is not associated with differential growth during this developmental window (Fig. 1D,G). Clones resulting from a single cell within the tooth area exhibit an average increase in surface area over 48 h that is twice the one of a sinus clone over the same time frame (Fig. 1E,H). To complete these analyses, we measured cell surface areas in sinuses and teeth at each time point, and found significantly smaller cells in sinuses (Fig. 1I). To further confirm these results and avoid potential bias resulting from time-lapse experiments, we looked at the distribution of cell surface areas in sinuses and teeth on independent 3D acquisitions of leaves from the same line, and plotted the results according to the width of the teeth. For leaves with a tooth one width below 100 µm, the mean cell surface areas were 48 µm² and 68 µm² in sinuses and teeth, respectively, whereas for a tooth one width between 100 µm and 200 µm, the mean cell surface areas reached 63 µm² in sinuses and 89 µm² in the tooth (Fig. 1J, Fig. S3). Altogether, these results indicate that early stages of teeth development result from a spatial difference in cell growth of dividing cells between regions of sinuses and teeth with a lower cell growth at sinuses.

CUC3 expression is located in very few cells exhibiting small surface areas at sinuses

To figure out the link between expression patterns of CUCs and differential growth occurring during leaf morphogenesis, we used 3D imaging on lines carrying transcriptional reporters for *CUC2* and *CUC3* (Fig. 2A). We first projected signal from *pCUC2::RFPer* and *pCUC3::CFPer* reporters onto the segmented surfaces of leaves (Fig. 2B,C). We then normalized mean projected signal intensities for both reporters and applied a threshold on these normalized signals to classify cells into three domains: *CUC2*-expressing cells; *CUC2*- and *CUC3*-expressing cells, named CUC2 and CUC2/3, respectively, hereafter; and cells expressing neither *CUC2* nor *CUC3*, assigned as noCUCs cells. In addition, the sinus defined on the gaussian curvature of the surface is outlined in yellow (Fig. 2D). The data show that whereas *CUC2* is expressed in a rather broad region comprising the sinus and surrounding cells, *CUC3* expression is far more restricted and tightly overlaps with the sinus. To gain insight into the distribution of cell surface areas within the CUC2 and CUC2/3 domains, the outlines of the corresponding expression domains were drawn on the cell surface area map (Fig. 2E) and the areas of individual cells within each domain was measured on 29 independent leaves of a similar developmental stage. These measurements revealed that the CUC2/3 domain is composed of smaller cells than *CUC2*-expressing cells, these CUC2 cells being smaller than cells expressing neither *CUC2* nor *CUC3* (Fig. 2F). Both map (Fig. 2E) and quantifications (Fig. 2F) revealed that cell-surface areas are more homogeneous in the CUC2/3 domain than in the CUC2 domain. These results, together with the phenotype of a smooth margin in both *cuc3-105* mutant or in transgenic lines exhibiting higher CUC2 activity in the *cuc3-105* background (Hasson et al., 2011; Maugarny-Cales et al., 2019), indicate that CUC3 is likely to be required for the local inhibition of cell growth at the margin during growth and development of serrations.

Development (2020) 147, dev183277. doi:10.1242/dev.183277

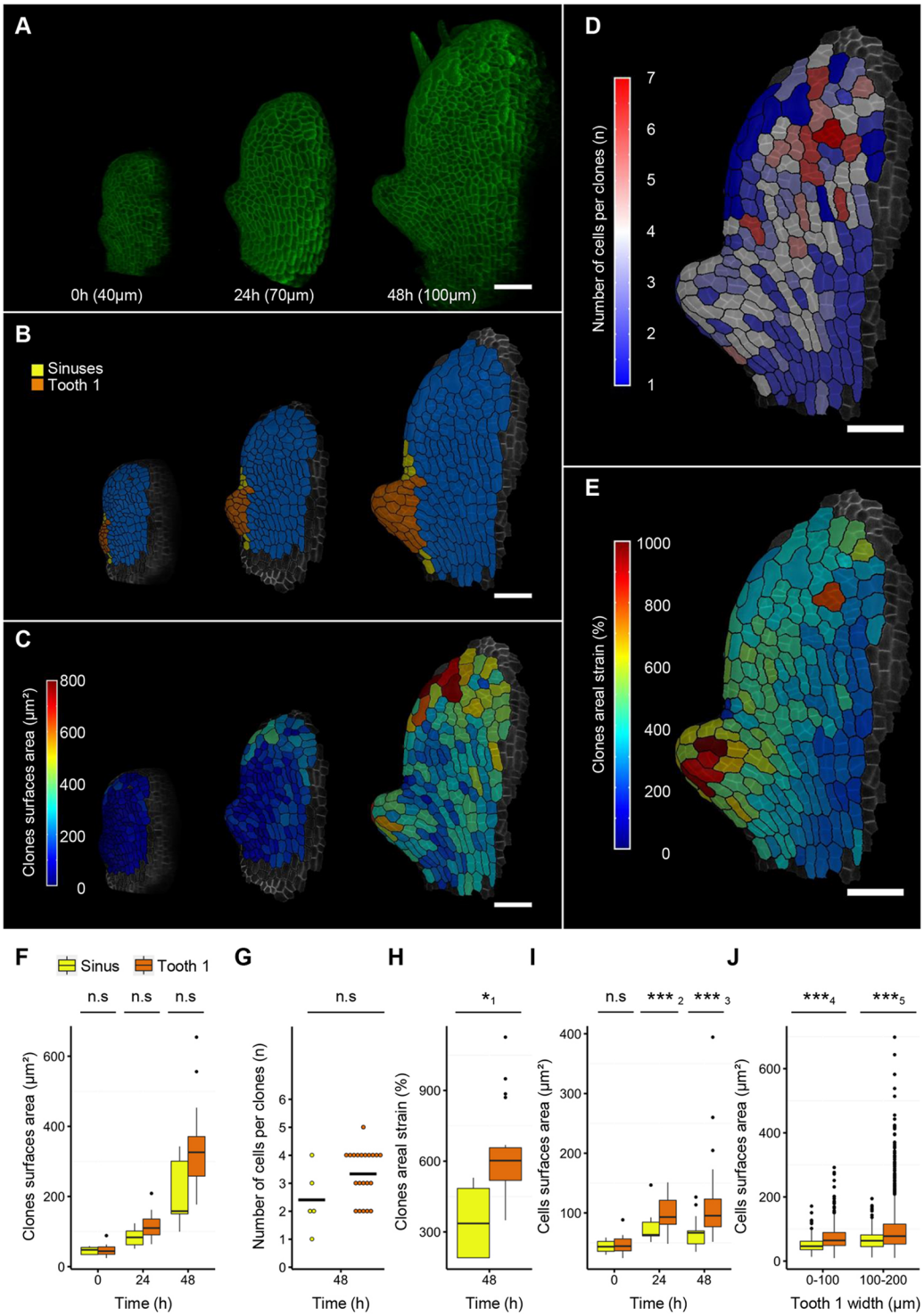

Fig. 1. Low cell growth at sinuses is responsible for teeth arising at the leaf margin. (A) Leaf primordia of a plasma membrane marker-expressing line (*p70s::PIP2-GFP*) at three time points of a time-lapse experiment (tooth 1 width is indicated under each image). (B) Segmented abaxial epidermis with clones deriving from cells at 0 h outlined in black and colored according to the type of clones (sinuses in yellow and tooth in orange) see Fig. S1 for the detailed method of clone type assessment. (C) Heatmaps of clone surface areas at each time point of the experiment. (D) Heatmap of proliferation over the 48 h of the experiment (number of cells per clone at the end of the experiment). (E) Heatmap of the clone areal strain over the 48 h of the experiment, defined as [(clone area at 48 h−clone area at 0 h)/clone area at 0 h]×100. (F) Distribution of clone surface areas by clone type for each time point of the experiment. (G) Numbers of cells formed per clone at the end of the experiment (individual data are represented by dots and mean is represented by a black line). (H) Area extension over the 48 h of the experiment for sinus and tooth clones. (I) Distribution of cell-surface areas in sinus and tooth at each time point of this time-lapse experiment. (J) Distribution of cell-surface areas in sinus and tooth according to the width of the tooth from a number of independent static acquisitions (data for this panel came from acquisitions of 32 and 23 independent Col-0 leaves with the tooth 1 width ranging between 0 and 100 µm or 100 and 200 µm, respectively, for a total of 283 and 237 sinus cells and 1384 and 2948 tooth cells). Scale bars: 50 µm in A-E. Asterisks represent statistical differences according to a *t*-test: **P*<0.05, ***P*<0.01, ****P*<0.001 ($*_1$=0.0148; $***_2$=0.0006; $***_3$=2.33e^{-06}; $***_4$=2.2e^{-16}; $***_5$=2.2e^{-16}). In F,H-J, boxes represent the inter quartile range, the segment inside the box shows the median value, whiskers above and below the box show the location of minimum and maximum. In G, the horizontal line represents the mean.

Development (2020) 147, dev183277. doi:10.1242/dev.183277

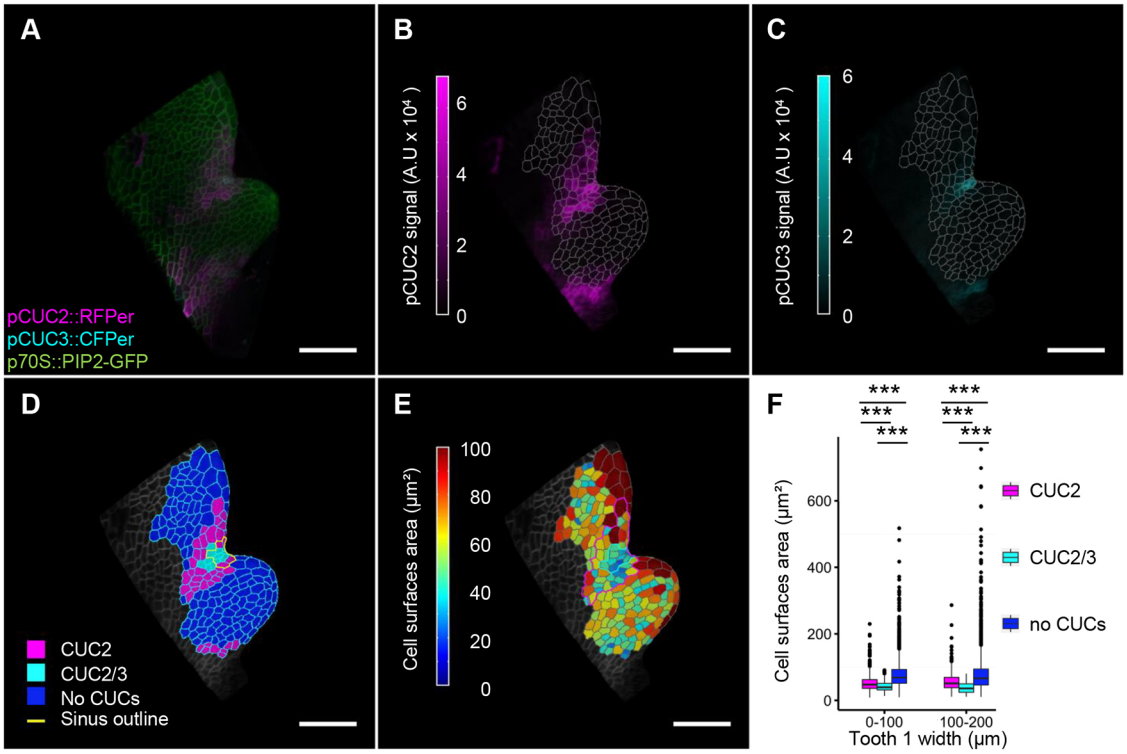

Fig. 2. The *CUC3* expression domain is associated with reduced cell areas. (A) Leaf primordia of a line co-expressing plasma membrane marker and reporters for *CUC2* and *CUC3* expression. (B) *CUC2* signal from the abaxial epidermis projected on the leaf surface. (C) *CUC3* signal from the abaxial epidermis projected on the leaf surface. (D) Map of cell expression types, based on the normalized projected signal of *CUC2* and *CUC3* cells are classified in CUC2 or CUC2 and CUC3 cells (CUC2 in magenta and CUC2/3 in cyan, remaining cells in blue). The yellow line outlines the sinus determined by the negative gaussian curvature. (E) Map of cell surface areas with the outline of *CUC2* (magenta line) and *CUC2/3* expression domains (cyan line). (F) Distribution of cell surface areas in CUC2, CUC2/3 and no CUCs domains, according to the width of tooth 1. Boxes represent the inter quartile range, the segment inside the box shows the median value, whiskers above and below the box show the location of minimum and maximum, and black dots represent the outliers of the distribution. Data for this plot come from acquisitions performed on 18 and 10 independent leaves with tooth 1 width ranging between 0 and 100 µm or 100 and 200 µm, respectively, corresponding to a total of 1035 and 336 *CUC2*-expressing cells, and 270 and 77 *CUC3*-expressing cells. Scale bars: 50 µm in A-E. Asterisks represent statistical differences according to a *t*-test: ***$P<2.2e^{-16}$.

The local reduction of cell growth at the sinuses is mediated by CUC3

To test this hypothesis, we introduced the *p70S::PIP2-GFP* plasma membrane marker in the *cuc3-105* mutant background and performed 3D imaging and time-lapse experiments on leaf primordia (Fig. 3). We applied the previously described pipeline (Fig. S1) to identify cells or derived clones from the tooth and its relative distal sinus. Data resulting from time-lapse experiments revealed that no division was observed in the very few cells identified as forming the sinus in *cuc3-105*, whereas a variable number of divisions occurred per clone in tooth (Fig. 3A,B,F). Within the same period, extension of clone surface area occurred in *cuc3-105* sinus and tooth domains (Fig. 3C,G), although weaker than the extension in clone surface areas in wild type within the same time frame (Fig. 1E,I). On a cellular scale, measurements of cell surface areas were performed on tooth and sinus cells after redefining the latter at each point of the time lapse on the basis of the gaussian curvature. An increase in cell surface area of about four times was measured at the sinus, whereas the mean cell surface areas remained constant in the tooth (Fig. 3H). Performing cell area analyses on a number of independent static acquisitions in *cuc3-105* confirmed the differences in cell surface areas between sinuses and teeth (Fig. 3I). Comparison of the distribution of cell surface areas in sinuses and teeth of *cuc3-105* with the ones in Col-0 indicates that, although cell surface areas in sinuses of *cuc3-105* are significantly higher than in Col-0 (Fig. 3J), there is no significant difference in tooth cell surface areas (Fig. 3K). These data suggest that CUC3 is somehow required to maintain cell division at the sinuses and is involved in local cell growth reduction at the sinus.

To further investigate the effect of CUC3 on cell growth, we generated an inducible line overexpressing *CUC3* in a *cuc3-105* background using the previously reported *p35S::CUC3-GR* construct (Bennett et al., 2010) (CUC3-GR hereafter) and performed dexamethasone (DEX) induction on seedlings cultivated *in vitro*. CUC3 induction triggers drastic changes in leaf morphology, including leaf hyponasty (data not shown) and enhanced serrations, compared with non-induced leaves. To visualize the associated changes at the cellular level, we performed 3D imaging on leaves stained with Calcofluor to segment and measure the surface areas of the epidermal cells at sinuses (Fig. 4A). The restoration of CUC3 activity in the region of sinuses is associated with cells exhibiting mean surface areas of 62 µm², while in non-induced conditions, mean cell surface areas in *cuc3-105* sinuses is 102 µm² (Fig. 4B). Cell areas in the region of the midvein are smaller than in *cuc3-105* (arrows in Fig. 4A), suggesting that ectopic expression of *CUC3* in this region also affects cell growth/expansion of these cells. However p35S-mediated expression of *CUC3* does not result in a homogenous reduction of cell size all over the leaf surface. Larger and rather isotropic cells are observed in a domed zone in the middle of the teeth and in the more distal domain of the leaf; however, this

Development (2020) 147, dev183277. doi:10.1242/dev.183277

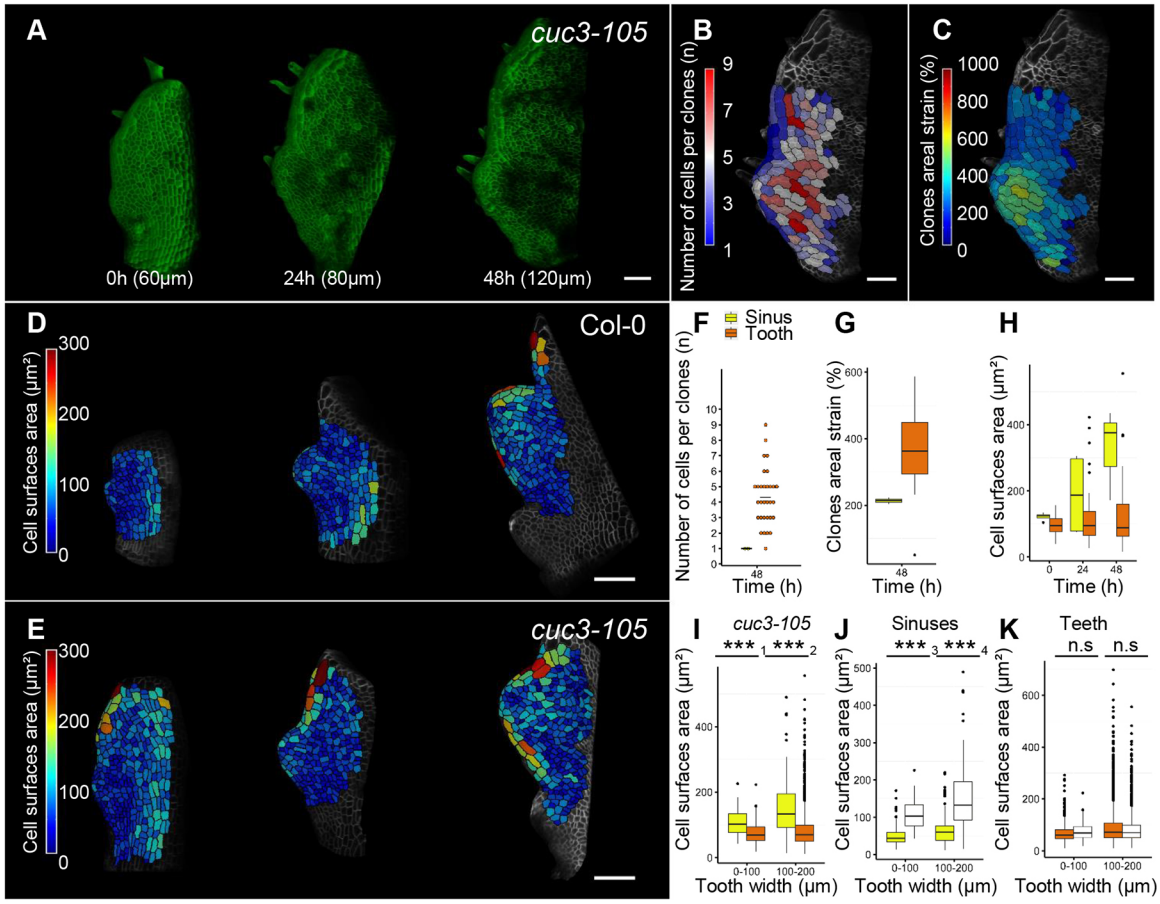

Fig. 3. *CUC3* mediates local cell growth reduction at the leaf margin. (A) 3D images of the same *cuc3-105* leaf primordia at three time points of a time-lapse experiment (tooth 1 width is indicated under each image). (B,C) Maps of the number of cells per clone and clone areal strain over the 48 h of the experiment (represented by the last time point of the experiment). (D,E) Maps of cell surface areas for three representative leaves of Col-0 and *cuc3-105* (tooth widths from left to right are ∼50 µm, ∼100 µm and 150 µm). (F) Number of cells per clone at the end of the experiment in sinus (yellow) and tooth (orange) regions (related to B). (G) Area extension of clones in sinus and tooth at the end of the experiment compared with time 0 (related to C). (H) Distribution of cell surface areas in sinuses and teeth at each time point of the experiment. Sinus cells are identified as such at each time based on the gaussian curvature. (I) Distribution of cell surface areas in *cuc3-105* sinuses and teeth according to the width of the tooth; data are pooled from acquisitions performed on 8 and 23 independent *cuc3-105* leaves with tooth 1 width ranging between 0 and 100 µm or 100 and 200 µm, respectively, for a total of 38 and 133 sinus cells and 286 and 2437 tooth cells. (J) Distribution of cell-surface areas in sinus cells of Col-0 (yellow) and *cuc3-105* (white) leaves according to the width of the tooth [data for *cuc3-105* sinus cells are the same as in I; data from acquisitions performed on 32 and 23 independent Col-0 leaves with tooth 1 width ranging between 0 and 100 µm or 100 and 200 µm have been pooled for this plot (data used in Fig. 1)]. (K) Distribution of cell-surface areas in teeth of Col-0 (orange) and *cuc3-105* (white) according to the width of the tooth (data for this plot came from the same acquisitions used in I and J). Scale bars: 50 µm. Statistical differences according to *t*-test: ****P*-value<0.001 ($***_1$ =3.994e^{-05}; $***_2$=2.283e^{-15}; $***_3$=7.552e^{-11}; $***_4$=3.503e^{-15}; n.s., not significant).

domain lacks the elongated cells forming the leaf margin (arrowheads in Fig. 4A). To further explore the influence of CUC3 on cell elongation, we induced *CUC3* expression in dark-grown seedlings and measured hypocotyl elongation, the growth of which is triggered almost exclusively by anisotropic expansion of pre-existing cells in the mature embryo (Gendreau et al., 1997). 48 h after germination, CUC3-GR hypocotyls grown in the presence of DEX exhibited an average length of 0.8 mm (Fig. 4C,E,G) while the non-induced hypocotyls reached 12 mm in mean length (Fig. 4D,F,G); *cuc3-105*, *p35S::TRANSPARENT TESTA 8-GR* in *tt8-1* (TT8-GR) and *tt8-1* control lines exhibited only weak variations of hypocotyl length after treatment with DEX (Fig. 4G). *CUC3* ectopic expression drastically suppresses cell elongation in hypocotyls grown in darkness, indicating that CUC3 is a negative regulator of both cell growth of cycling cells and cell expansion.

Smoothening of tooth 1 at later stages of leaf development is associated with a release of CUC3 mediated cell growth inhibition at the sinus

In the later stages of leaf development, the first pair of teeth tends to be smoothed in wild-type plants, indicating that the initial differential growth is not further maintained (Biot et al., 2016). A change in differential growth might be the consequence of a change in cell growth behavior of sinuses cells. As CUC3 was involved in the local reduction of cell growth at sinuses in the first stages of serration formation, we questioned whether cell growth dynamics and *CUC3* expression change in sinuses during tooth 1 smoothening. We performed time-lapse experiments at late stages of teeth development in Col-0 co-expressing a plasma membrane marker and a transcriptional reporter for *CUC3* (*p70S::PIP2-GFP/pCUC3::CFPer*). We focused our analyses on sinus cells identified as described above (Fig. S1), we measured cell surface areas, numbers

Development (2020) 147, dev183277. doi:10.1242/dev.183277

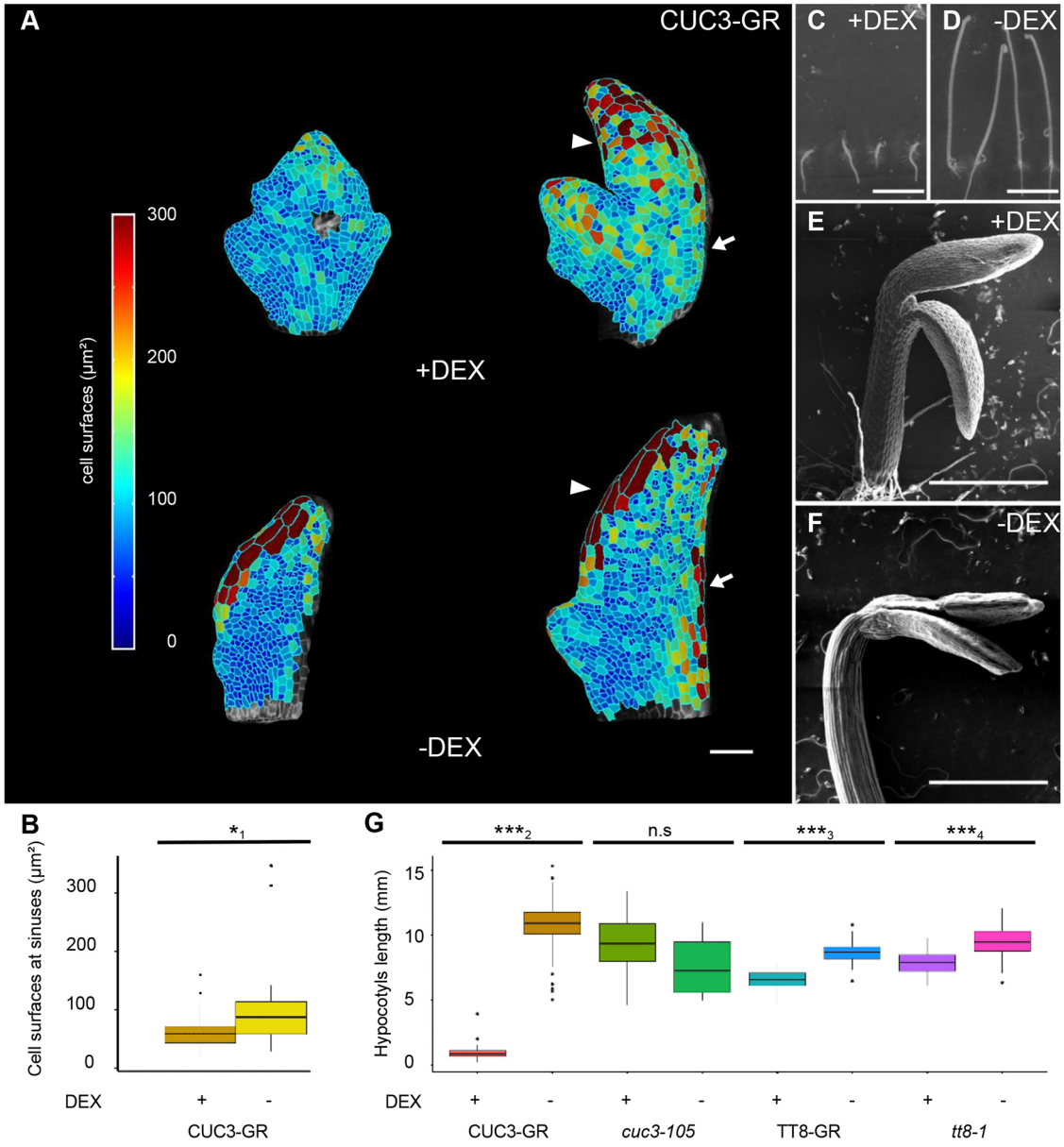

Fig. 4. *CUC3* represses cell growth. (A) Map of cell surfaces for representative leaves of *cuc3-105* carrying the *p35S::CUC3-GR* transgene in DEX-induced or non-induced conditions (cell outlines are visualized with Calcofluor staining). (B) Cell-surface area distribution at sinuses in induced or non-induced conditions; data result from acquisitions performed on four independent leaves per condition with tooth 1 width ranging from 40 to 140 µm corresponding to a total of 44 and 25 sinus cells for DEX-treated and untreated samples. (C) 48 h DEX-induced dark-grown seedlings of *p35S::CUC3-GR cuc3-105* exhibiting short hypocotyls. (D) 48 h non-induced dark-grown seedlings of *p35S::CUC3-GR cuc3-105* hypocotyls. (E,F) Scanning electron microscopy images of a DEX-induced (E) and a non-induced (F) dark-grown seedling. (G) Distributions of *p35S::CUC3-GR cuc3-105*, *cuc3-105*, *p35S::TT8-GR tt8-1* and *tt8-1* hypocotyl lengths under DEX-induced and non-induced conditions (*n*, numbers of hypocotyls measured per condition: CUC3-GR +DEX (*n*=121)/−DEX (*n*=175); *cuc3-105* +DEX (*n*=35)/−DEX (*n*=8); TT8-GR +DEX (*n*=29)/−DEX (*n*=39); *tt8-1* +DEX (*n*=38)/−DEX (*n*=31). Scale bars: 50 µm in A; 5 mm in C,D; 200 µm in E,F. Statistical differences according to *t*-test: **P*<0.05; ***P*<0.01; ****P*<0.001 ($*_1$=0.01624; $***_2$<2.2e^{-16}; $***_3$=9.276e^{-16}; $***_4$=1.194e^{-06}). In B and G, boxes represent the interquartile range, the segment inside the box shows the median value, whiskers above and below the box show the location of minimum and maximum, and black dots represent the outliers of the distribution.

of cells formed per clones and *pCUC3* projected signal at each time of the experiment (Fig. 5). Heat maps and measurement of cell-surface areas revealed that cell growth occurs in sinus cells (Fig. 5A,E). The absence of cell division in sinuses (Fig. 5B) indicates that this increase in cell-surface areas results from cell expansion. *pCUC3*-projected signal intensity (Fig. 5C) decreases over time as the cells expand in sinuses (Fig. 5D,F). These results are further confirmed by the measurements of sinus cell areas and *pCUC3*-projected signal on independent static acquisitions (Fig. 5G,H). These results indicate that growth at the sinus results solely from an increase in cell surface areas that strongly correlates with a decrease in *CUC3* expression during late stages of teeth development.

DISCUSSION

Spatial and temporal control of cell growth directs leaf serration

Serration initiation at the leaf margin is an example of differential growth. As this process takes place in the basal half of the leaf in a

Development (2020) 147, dev183277. doi:10.1242/dev.183277

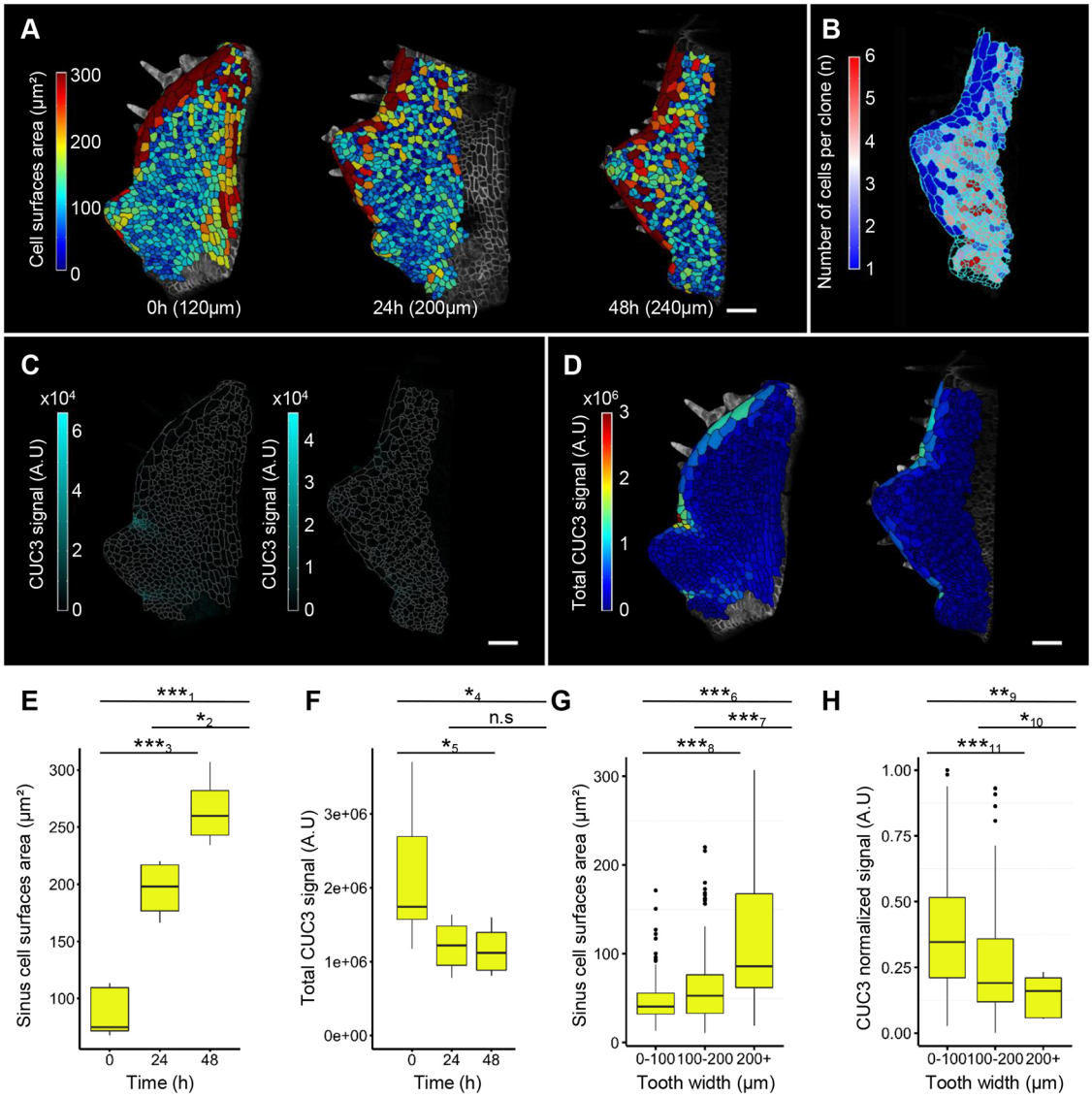

Fig. 5. Decrease in *CUC3* expression releases local restriction of sinus cell growth in late stages of teeth development. (A) Segmented leaf abaxial epidermis at three time points of a time lapse experiment (tooth 1 width is indicated under each image). (B) Heatmap of proliferation over 48 h of the experiment (number of cells per clone at the end of the time lapse). (C) *CUC3* signal from the epidermis projected onto the leaf surface. (D) Heatmaps of total *CUC3* signal per cell at the beginning and end of the time lapse. (E,F) Distribution of cell-surface areas (E) and *CUC3* signal (F) at each time point of this time lapse experiment. (G,H) Distribution of cell-surface area (G) and *CUC3* normalized signal (H) from sinuses of teeth 1 of distinct width (acquisitions were performed on 44 independent leaves for a total of 376 sinuses cells). Scale bars: 50 µm. **P*<0.05; ***P*<0.01; ****P*<0.001 based on *t*-test ($^{***}_1$=3.278e^{-4}; $^{*}_2$=0.01682; $^{***}_3$=7.894e^{-4}; $^{*}_4$=0.03024; $^{*}_5$=0.03892; $^{***}_6$=6.311e^{-4}; $^{***}_7$=0.00459; $^{***}_8$=2.957e^{-5}; $^{***}_9$=0.001347; $^{*}_{10}$=0.04468; $^{***}_{11}$=2.988e^{-5}). In E-H, boxes represent the interquartile range, the segment inside the box shows the median value, whiskers above and below the box show the location of minimum and maximum, and black dots represent the outliers of the distribution.

population of proliferating cells, the spatial differences in growth might rely on spatial differences in cell division or in cell growth. Time-lapse analyses provide information at several levels: clone area extension and clone surface areas informed us about clone growth, whereas the map of the number of cells per clones is directly related to cell division events. The combination of time-lapse experiments with the analysis of cell areas from numerous independent static acquisitions allowed us to determine the sequence of cellular events occurring from the initiation of the first tooth to its smoothening at a later stage of leaf development. In the first steps of tooth development (less than 100 µm in width) an equivalent number of cells are formed per clone in sinus and tooth, whereas clone areal strain and clone areas are higher in tooth than in sinuses (Fig. 1 and Fig. S2). These results, confirmed by the measurement of smaller cells in the sinus on static acquisitions, clearly indicate that differences of cell growth between sinus and tooth are responsible for the differential growth in the initial phase of tooth outgrowth. This is in accordance with previous studies reporting small cells in sinuses of *Arabidopsis* leaves and inter-leaflets regions of tomato leaves (Kawamura et al., 2010; Rossmann et al., 2015). It is also in accordance with the recently reported data showing reduced area extension in *A. thaliana* sinuses and inter-leaflets regions of *C. hirsuta* leaves (Kierzkowski et al., 2019; Vlad et al., 2014). Later on (between 100 and 200 µm of tooth width, Fig. S3), the number of cell divisions is reduced in the region of the sinus. At this stage, growth of clones no longer differs between sinus and tooth. However, as homogeneous growth takes place on cells in different areas, the difference in cell-surface areas between

Development (2020) 147, dev183277. doi:10.1242/dev.183277

sinus and serration is maintained (Fig. S3). When the tooth reaches more than 200 µm in width, cell division stops and increased cell expansion takes place in the distal sinus (Fig. 5), potentially requiring endoreplication that has been reported to support an enhanced increase in cell size prior to differentiation (Beemster et al., 2005). Such a decrease and even arrest of cell division at the latest stages might be correlated with the progressive retreat of the cell division front in the whole leaf (Andriankaja et al., 2012; Donnelly et al., 1999; Fox et al., 2018). Our results reveal the crucial importance of fine spatial and temporal control of cell growth to sustain dynamic changes of leaf shape in *A. thaliana*.

Very localized repression of cell growth by CUC3 maintains leaf serration

Our results show that *CUC3* expression is restricted to a very limited number of sinus cells that are smaller than the surrounding cells (Fig. 2). In addition, measurements of cell surface areas on the *cuc3-105* mutant or CUC3 overexpression lines support the theory that CUC3 acts as a negative regulator of cell growth (Figs 3 and 4). This is reinforced by the observation that the decrease in *CUC3* expression in a late stage of teeth development correlates with an increase in cell surface area at the sinus (Fig. 5). This negative and local regulation of cell growth by CUC3 might represent a local differentiation delay that would be consistent with the roles of CUC genes in maintaining meristematic identity (Hibara et al., 2003). To our knowledge, the only other negative regulator of cell growth involved in leaf margin morphogenesis is *RCO*, which is expressed in *C. hirsuta* leaves but is not present in *A. thaliana* (Kierzkowski et al., 2019; Vlad et al., 2014). The strong reduction of cell growth imputed to CUC3 might, however, involve a synergic effect of CUC2 and CUC3, as it has been shown that they could form heterodimers (Gonçalves et al., 2015; Rubio-Somoza et al., 2014). However, conditional overexpression of *CUC3* prevents tooth smoothening (Fig. 4), indicating that CUC3 is sufficient to maintain the repression of cell growth/expansion at the sinus. *CUC3* expression has been reported to be induced upon mechanical stress (Fal et al., 2016), and the initiation of differential growth by CUC2 (Bilsborough et al., 2011; Maugarny-Cales et al., 2019) produces an increase in mechanical stress level at the leaf margin. These two mechanisms provide an efficient combination that can induce the expression of *CUC3* very locally at the sinus at a very early stage of tooth initiation and is an effective feedback mechanism that reinforces and maintains differential growth. Even if the growth and mechanical properties of sinus cells are mainly controlled at the local level by the differential growth between sinuses and teeth, it is likely that the evolution of the growth pattern at the level of organs also interferes with local mechanical stress pattern. Growth pattern at the leaf level can direct a mechanical stress pattern similar to that reported in sepals (Hervieux et al., 2016). The overall organ growth and the resulting stress pattern could release the mechanical stress at the leaf margin, especially in sinus cells, and then trigger the decrease in *CUC3* expression in late stages of teeth development. The dynamics of *CUC3* expression have a strong impact on leaf morphogenesis, despite its very localized expression.

In conclusion, we described a differential growth process occurring in a population of proliferating cells in young leaves. Like differential growth occurring in apical hook formation or tropic responses, it relies on the temporal and spatial control of cell growth of small groups of cells. At the leaf margin, it involves differential distribution of the CUC3 transcription factor that negatively controls cell growth. This negative control necessarily involves a modulation in the expression of growth-related genes, among which cell wall remodeling genes are likely to be potential targets. Identification of these genes will require transcriptional analyses of sinus cells compared with others, which might be rather difficult to perform; however, single cell analyses are now emerging and might provide novel perspectives (Denyer et al., 2019; Ryu et al., 2019; Zhang et al., 2019). Identifying CUC3 targets in the context of leaf serrations would be an important step towards understanding the molecular mechanisms underlying differential growth and growth control at boundary domains.

MATERIALS AND METHODS

Plant materials and growth conditions

All lines are in the Columbia-0 (Col-0) ecotype, the *cuc3-105* mutant is described elsewhere (Hibara et al., 2006), *pCUC3::CFPer* and *pCUC2::RFPer* have been described previously (Gonçalves et al., 2015), *p70s::PIP2-GFP* have been described previously (Luu et al., 2012), the tt8-1 mutant have been described previously (Nesi et al., 2001) and *p35S::TT8-GR* in *tt8-1* background have been described previously (Baudry et al., 2004). The *p35S::CUC3-GR* construct have been described previously (Bennett et al., 2010) and was introduced by transformation in *cuc3-105*. Seeds were surface sterilized (10 min in 70% ethanol, SDS 0.5%, then washed for a few seconds in 95% ethanol and dried) prior to being sown on half Murashige and Skoog medium in 0.8% agar, pH adjusted at 5.7. All plates were stratified at 4°C for 48 h. All plants were grown for 7 days *in vitro* in long-day photoperiods (16 h light/8 h dark at 21°C) before being transferred to soil under short-day photoperiods [1 h dawn (19°C, 65% hygrometry, 80 µmol m^{-2} s^{-1} light), 6 h day (21°C, 65% hygrometry, 120 µmol m^{-2} s^{-1} light), 1 h dusk (20°C, 65% hygrometry, 80 µmol m^{-2} s^{-1} light), 16 h dark (18°C, 65% hygrometry, no light)] for 14 days.

Culture conditions for time-lapse imaging

Plants were carefully removed from soil, and cotyledons and leaves 1 to 10 were removed using fine tweezers and surgical syringe needle under a stereo microscope. Seedlings were then transferred onto a plate containing half Murashige and Skoog media (MS/2) supplemented with 1% sucrose and 0.8% agarose. Dissected seedlings were glued to the media by careful deposition of agarose droplets on the hypocotyls. Samples were then imaged every 24 h and grown under long-day conditions between imaging sessions.

Dexamethasone *in vitro* inductions

Surface-sterilized seeds were sown on MS1/2 and cultivated vertically in standard long day conditions for 7 days, seedlings were then transferred on MS1/2 supplemented with 10 µM dexamethasone or 0.1% ethanol (mock condition) and cultivated for another 7 days. For hypocotyl growth experiments, seeds were sown directly on plates containing 10 µM dexamethasone or 0.1% ethanol as a mock treatment. After stratification, plates were exposed to light for 4 h then were transferred vertically in darkness at 24°C for up to 7 days.

Sample preparation and confocal imaging

In order to visualize the cell edge in a line not carrying a plasma membrane marker, dissected leaves were stained using Calcofluor 0.1% (in distillated water) for 24 h prior to being mounted between slide and coverslip in Citifluor mounting media. For all the other experiments, samples were prepared as for time-lapse acquisition. Prior to imaging, samples were immersed in water for 5 min in order to saturate the agarose gel and avoid uncontrolled movement during imaging. Acquisitions were performed on an upright Leica TCS SP8 laser scanning confocal microscope equipped with a long distance water immersion lens (Leica, 40X0, 8NA water HCX APO L). Calcofluor and CFP were exited at 405 nm, GFP at 488 nm, VENUS at 514 nm and RFP at 560 nm. Calcofluor and CFP signal were collected from 415 to 480 nm, GFP from 498 nm to 510 nm, VENUS from 524 nm to 554 nm and RFP from 570 nm to 650 nm. GFP was collected using a Hyd detector, fluorescence from the other fluorochromes or dyes was collected using PMT detectors. Sequential image settings were used when required. All samples were acquired as a stack of images with a voxel resolution of about 0.5×0.5×0.5 µm.

Development (2020) 147, dev183277. doi:10.1242/dev.183277

Image analyzes

Hypocotyl length measurements were performed using NeuronJ plug-in (/imagescience.org/meijering/softwareneuronj/) of ImageJ (imagej.nih.gov/ij/) and data exported to R software (www.r-project.org/) for further analyses. All stacks of images were processed using MorphoGraphX (MGX) software (Barbier de Reuille et al., 2015) (www.mpipz.mpg.de/MorphoGraphX/software) to segment cells, perform lineage tracking and measure growth parameters; quantitative data were then exported to R as .csv files to perform further analyses. These methods are provided in brief as follows.

Cell segmentation

A stack of images stored in a single .tiff was loaded into MGX, a Gaussian blur was applied to the entire stack within a neighborhood of 0.3 µm and a global solid shape of the leaf primordia was then extracted using the Edge detect process. Parts of the stack not needed for further analyses were removed using the pixel editor. A mesh of the leaf primordia surface was then created using marching cubes of 5 µm side length. The mesh was then smoothed and subdivided. Once the surface of the leaf primordia had been extracted, plasma membrane signal from the epidermis layer was projected onto the surface over a range of 2 to 6 µm from the surface. Seeds were manually added to every cell, the surface signal was then blurred using signal Gaussian blur function in a neighborhood of 1 µm and segmentation was carried out using watershed algorithm. To refine the segmentation, the mesh was subdivided at the cell edge, signal projected onto the refined mesh and watershed run again.

Lineage tracking

After images of all the time points of an experiment were segmented using the cell segmentation pipelines, the first two consecutive time points of an experiment were loaded into MGX as segmented mesh files. The mesh of the first time point was scaled to be the same size as the mesh of the second time point. The mesh of the first time point was then aligned over the mesh of the second time point to make the cell outlines locally coincident. Labels from the first time point were then transferred to the second time point by clicking on the center of the corresponding cells. If a cell had undergone division between the two time points, the same parent label was given to the two daughter cells. Once this operation was achieved for the first two time points, it was repeated to transfer the label from the second time point to the last time point. These new labelings are saved as parent labels.

Cells and growth parameter measurements

Once segmented mesh was obtained, cell surface area and mean Gaussian curvature of the surface were measured for each cell. After cell lineage was completed, the number of cells formed per clones over 48 h was extracted. Clone areal strain was measured as follows: $[(\text{clone area}_{\text{at } 48h} - \text{clone area}_{\text{at } 0h})/\text{clone area}_{\text{at } 0h}] \times 100$.

Classification of cells

Classification of cells into CUC2, CUC2/3 or no CUCs categories in Fig. 2. Signals from *pCUC2::RFPer* or *pCUC3::CFPer* were projected onto a segmented mesh using the project signal function over a range of 2 to 6 µm from the surface. Mean signal intensities were collected for both reporters in each cells. A .csv file containing these data was exported to R software. Cell signal intensities from all the acquisitions on lines expressing these reporters were pooled together in order to plot the overall distribution of signal intensities according to the surface of cells for both reporters. Signal intensities were normalized in order to range the signal intensity values between 0 and 1. A threshold was applied for both signals: all cells with a normalized signal over 0.2 were considered as expressing the reporter. Cells were then classified into CUC2, CUC2/3 or noCUCs according to the reporter they expressed after the previous steps of the pipeline. After cell classification, cell areas, area of domain (CUC2, CUC2/3 and no CUCs) as well as number of cells per domain were computed from the data files on R.

For each acquisition, a single .csv file was generated as an output of R data analyses pipelines. It contains all the relevant information on cells: classification into marker domains, cell area, mean gaussian curvature, localization (sinus, tooth and leaf). These files can be read in MorphoGraphX in order to visualize any quantified information on the surface mesh of the acquisition. Tooth width corresponds to the distance between two consecutive sinuses.

For time-lapse experiments, additional .csv files were generated. They contain additional information on: clones area, numbers of cells per clones, area extension and clone position (distal sinus, tooth and leaf).

Acknowledgements

This work was achieved by the transcription factor and architecture team headed by P. Laufs at IJPB Versailles and benefited from available genetic and molecular tools, technical skills and scientific discussions within the whole team, with special acknowledgments to Nicolas Arnaud and Patrick Laufs for critical reading of the manuscript. We thank Pradeep Das, Anna-Maria Kiss and Christophe Godin (RDP, Lyon) for helpful discussions, and Teva Vernoux (RDP, Lyon) for critical reading of the manuscript. We warmly thank Carlos Galvan Ampudia, Géraldine Burnoud (RDP Lyon) and Katia Belcram (IJPB, Versailles) for technical advice. We thank Ben Scheres, who kindly provided the *p35S::CUC3-GR* construct, and Loic Lepiniec (IJPB, Versailles) for providing TT8-GR and *tt8-1* lines. We also pay tribute to Olivier Grandjean, whose advice was invaluable in setting up the time-lapse experiments. We are grateful to the members of the IJPB plant culture service who took care of the plants.

Competing interests

The authors declare no competing or financial interests.

Author contributions

Conceptualization: L.S., C.P.-R.; Methodology: L.S.; Validation: L.S.; Formal analysis: L.S.; Investigation: L.S.; Writing - original draft: L.S., C.P.-R.; Supervision: C.P.-R.; Project administration: C.P.-R.; Funding acquisition: C.P.-R.

Funding

This work and L.S. were supported by the Agence Nationale de la Recherche (ANR-14-CE11-0018). The IJPB benefits from the support of the LabEx Saclay Plant Sciences-SPS (ANR-10-LABX-0040-SPS).

Supplementary information

Supplementary information available online at
http://dev.biologists.org/lookup/doi/10.1242/dev.183277.supplemental

References

Aida, M. and Tasaka, M. (2006). Morphogenesis and patterning at the organ boundaries in the higher plant shoot apex. *Plant Mol. Biol.* **60**, 915-928. doi:10.1007/s11103-005-2760-7

Aida, M., Ishida, T., Fukaki, H., Fujisawa, H. and Tasaka, M. (1997). Genes involved in organ separation in Arabidopsis: an analysis of the cup-shaped cotyledon mutant. *Plant Cell* **9**, 841-857. doi:10.1105/tpc.9.6.841

Aida, M., Ishida, T. and Tasaka, M. (1999). Shoot apical meristem and cotyledon formation during Arabidopsis embryogenesis: interaction among the CUP-SHAPED COTYLEDON and SHOOT MERISTEMLESS genes. *Development* **126**, 1563-1570.

Andriankaja, M., Dhondt, S., De Bodt, S., Vanhaeren, H., Coppens, F., De Milde, L., Muhlenbock, P., Skirycz, A., Gonzalez, N., Beemster, G. T. et al. (2012). Exit from proliferation during leaf development in Arabidopsis thaliana: a not-so-gradual process. *Dev. Cell* **22**, 64-78. doi:10.1016/j.devcel.2011.11.011

Barbier de Reuille, P., Routier-Kierzkowska, A. L., Kierzkowski, D., Bassel, G. W., Schupbach, T., Tauriello, G., Bajpai, N., Strauss, S., Weber, A., Kiss, A. et al. (2015). MorphoGraphX: a platform for quantifying morphogenesis in 4D. *Elife* **4**, 05864. doi:10.7554/eLife.05864

Baudry, A., Heim, M. A., Dubreucq, B., Caboche, M., Weisshaar, B. and Lepiniec, L. (2004). TT2, TT8, and TTG1 synergistically specify the expression of BANYULS and proanthocyanidin biosynthesis in Arabidopsis thaliana. *Plant J.* **39**, 366-380. doi:10.1111/j.1365-313X.2004.02138.x

Beemster, G. T. S., De Veylder, L., Vercruysse, S., West, G., Rombaut, D., Van Hummelen, P., Galichet, A., Gruissem, W., Inzé, D. and Vuylsteke, M. (2005). Genome-wide analysis of gene expression profiles associated with cell cycle transitions in growing organs of Arabidopsis. *Plant Physiol.* **138**, 734-743. doi:10.1104/pp.104.053884

Bennett, T., van den Toorn, A., Sanchez-Perez, G. F., Campilho, A., Willemsen, V., Snel, B. and Scheres, B. (2010). SOMBRERO, BEARSKIN1, and BEARSKIN2 regulate root cap maturation in Arabidopsis. *Plant Cell* **22**, 640-654. doi:10.1105/tpc.109.072272

Berger, Y., Harpaz-Saad, S., Brand, A., Melnik, H., Sirding, N., Alvarez, J. P., Zinder, M., Samach, A., Eshed, Y. and Ori, N. (2009). The NAC-domain transcription factor GOBLET specifies leaflet boundaries in compound tomato leaves. *Development* **136**, 823-832. doi:10.1242/dev.031625

Bilsborough, G. D., Runions, A., Barkoulas, M., Jenkins, H. W., Hasson, A., Galinha, C., Laufs, P., Hay, A., Prusinkiewicz, P. and Tsiantis, M. (2011).

Model for the regulation of Arabidopsis thaliana leaf margin development. *Proc. Natl. Acad. Sci. USA* **108**, 3424-3429. doi:10.1073/pnas.1015162108

Biot, E., Cortizo, M., Burguet, J., Kiss, A., Oughou, M., Maugarny-Calès, A., Gonçalves, B., Adroher, B., Andrey, P., Boudaoud, A. et al. (2016). Multiscale quantification of morphodynamics: MorphoLeaf software for 2D shape analysis. *Development* **143**, 3417-3428. doi:10.1242/dev.134619

Blein, T., Pulido, A., Vialette-Guiraud, A., Nikovics, K., Morin, H., Hay, A., Johansen, I. E., Tsiantis, M. and Laufs, P. (2008). A conserved molecular framework for compound leaf development. *Science* **322**, 1835-1839. doi:10.1126/science.1166168

Denyer, T., Ma, X., Klesen, S., Scacchi, E., Nieselt, K. and Timmermans, M. C. P. (2019). Spatiotemporal developmental trajectories in the arabidopsis root revealed using high-throughput single-cell RNA sequencing. *Dev. Cell* **48**, 840-852.e845. doi:10.1016/j.devcel.2019.02.022

Donnelly, P. M., Bonetta, D., Tsukaya, H., Dengler, R. E. and Dengler, N. G. (1999). Cell cycling and cell enlargement in developing leaves of Arabidopsis. *Dev. Biol.* **215**, 407-419. doi:10.1006/dbio.1999.9443

Dumais, J. and Kwiatkowska, D. (2002). Analysis of surface growth in shoot apices. *Plant J.* **31**, 229-241. doi:10.1046/j.1365-313X.2001.01350.x

Fal, K., Landrein, B. and Hamant, O. (2016). Interplay between miRNA regulation and mechanical stress for CUC gene expression at the shoot apical meristem. *Plant Signal. Behav.* **11**, e1127497. doi:10.1080/15592324.2015.1127497

Fleming, A. J. (2018). Cellular architecture: regulation of cell size, cell shape and organ initiation. In *Annual Plant Reviews Online*, pp. 1-22 (ed. J. A. Roberts). Wiley.

Fox, S., Southam, P., Pantin, F., Kennaway, R., Robinson, S., Castorina, G., Sánchez-Corrales, Y. E., Sablowski, R., Chan, J., Grieneisen, V. et al. (2018). Spatiotemporal coordination of cell division and growth during organ morphogenesis. *PLoS Biol.* **16**, e2005952. doi:10.1371/journal.pbio.2005952

Galbiati, F., Sinha Roy, D., Simonini, S., Cucinotta, M., Ceccato, L., Cuesta, C., Simaskova, M., Benkova, E., Kamiuchi, Y., Aida, M. et al. (2013). An integrative model of the control of ovule primordia formation. *Plant J.* **76**, 446-455. doi:10.1111/tpj.12309

Gendreau, E., Traas, J., Desnos, T., Grandjean, O., Caboche, M. and Hofte, H. (1997). Cellular basis of hypocotyl growth in Arabidopsis thaliana. *Plant Physiol.* **114**, 295-305. doi:10.1104/pp.114.1.295

Gonçalves, B., Hasson, A., Belcram, K., Cortizo, M., Morin, H., Nikovics, K., Vialette-Guiraud, A., Takeda, S., Aida, M., Laufs, P. et al. (2015). A conserved role for CUP-SHAPED COTYLEDON genes during ovule development. *Plant J.* **83**, 732-742. doi:10.1111/tpj.12923

Hasson, A., Plessis, A., Blein, T., Adroher, B., Grigg, S., Tsiantis, M., Boudaoud, A., Damerval, C. and Laufs, P. (2011). Evolution and diverse roles of the CUP-SHAPED COTYLEDON genes in Arabidopsis leaf development. *Plant Cell* **23**, 54-68. doi:10.1105/tpc.110.081448

Hay, A., Kaur, H., Phillips, A., Hedden, P., Hake, S. and Tsiantis, M. (2002). The gibberellin pathway mediates KNOTTED1-type homeobox function in plants with different body plans. *Curr. Biol.* **12**, 1557-1565. doi:10.1016/S0960-9822(02)01125-9

Heisler, M. G., Ohno, C., Das, P., Sieber, P., Reddy, G. V., Long, J. A. and Meyerowitz, E. M. (2005). Patterns of auxin transport and gene expression during primordium development revealed by live imaging of the Arabidopsis inflorescence meristem. *Curr. Biol.* **15**, 1899-1911. doi:10.1016/j.cub.2005.09.052

Hervieux, N., Dumond, M., Sapala, A., Routier-Kierzkowska, A. L., Kierzkowski, D., Roeder, A. H., Smith, R. S., Boudaoud, A. and Hamant, O. (2016). A mechanical feedback restricts sepal growth and shape in arabidopsis. *Curr. Biol.* **26**, 1019-1028. doi:10.1016/j.cub.2016.03.004

Hibara, K., Takada, S. and Tasaka, M. (2003). CUC1 gene activates the expression of SAM-related genes to induce adventitious shoot formation. *Plant J.* **36**, 687-696. doi:10.1046/j.1365-313X.2003.01911.x

Hibara, K., Karim, M. R., Takada, S., Taoka, K., Furutani, M., Aida, M. and Tasaka, M. (2006). Arabidopsis CUP-SHAPED COTYLEDON3 regulates postembryonic shoot meristem and organ boundary formation. *Plant Cell* **18**, 2946-2957. doi:10.1105/tpc.106.045716

Kawamura, E., Horiguchi, G. and Tsukaya, H. (2010). Mechanisms of leaf tooth formation in Arabidopsis. *Plant J.* **62**, 429-441. doi:10.1111/j.1365-313X.2010.04156.x

Kierzkowski, D., Runions, A., Vuolo, F., Strauss, S., Lymbouridou, R., Routier-Kierzkowska, A. L., Wilson-Sanchez, D., Jenke, H., Galinha, C., Mosca, G. et al. (2019). A growth-based framework for leaf shape development and diversity. *Cell* **177**, 1405-1418.e1417. doi:10.1016/j.cell.2019.05.011

Kwiatkowska, D. (2004). Surface growth at the reproductive shoot apex of Arabidopsis thaliana pin-formed 1 and wild type. *J. Exp. Bot.* **55**, 1021-1032. doi:10.1093/jxb/erh109

Luu, D.-T., Martinière, A., Sorieul, M., Runions, J. and Maurel, C. (2012). Fluorescence recovery after photobleaching reveals high cycling dynamics of plasma membrane aquaporins in Arabidopsis roots under salt stress. *Plant J.* **69**, 894-905. doi:10.1111/j.1365-313X.2011.04841.x

Maugarny-Calès, A., Cortizo, M., Adroher, B., Borrega, N., Goncalves, B., Brunoud, G., Vernoux, T., Arnaud, N. and Laufs, P. (2019). Dissecting the pathways coordinating patterning and growth by plant boundary domains. *PLoS Genet.* **15**, e1007913. doi:10.1371/journal.pgen.1007913

Nesi, N., Jond, C., Debeaujon, I., Caboche, M. and Lepiniec, L. (2001). The Arabidopsis TT2 gene encodes an R2R3 MYB domain protein that acts as a key determinant for proanthocyanidin accumulation in developing seed. *Plant Cell* **13**, 2099-2114. doi:10.1105/TPC.010098

Perrot-Rechenmann, C. (2010). Cellular responses to auxin: division versus expansion. *Cold Spring Harb. Perspect Biol.* **2**, a001446. doi:10.1101/cshperspect.a001446

Piazza, P., Bailey, C. D., Cartolano, M., Krieger, J., Cao, J., Ossowski, S., Schneeberger, K., He, F., de Meaux, J., Hall, N. et al. (2010). Arabidopsis thaliana leaf form evolved via loss of KNOX expression in leaves in association with a selective sweep. *Curr. Biol.* **20**, 2223-2228. doi:10.1016/j.cub.2010.11.037

Reinhardt, D., Mandel, T. and Kuhlemeier, C. (2000). Auxin regulates the initiation and radial position of plant lateral organs. *Plant Cell* **12**, 507-518. doi:10.1105/tpc.12.4.507

Reinhardt, D., Pesce, E.-R., Stieger, P., Mandel, T., Baltensperger, K., Bennett, M., Traas, J., Friml, J. and Kuhlemeier, C. (2003). Regulation of phyllotaxis by polar auxin transport. *Nature* **426**, 255-260. doi:10.1038/nature02081

Rossmann, S., Kohlen, W., Hasson, A. and Theres, K. (2015). Lateral suppressor and Goblet act in hierarchical order to regulate ectopic meristem formation at the base of tomato leaflets. *Plant J.* **81**, 837-848. doi:10.1111/tpj.12782

Rubio-Somoza, I., Zhou, C.-M., Confraria, A., Martinho, C., von Born, P., Baena-Gonzalez, E., Wang, J.-W. and Weigel, D. (2014). Temporal control of leaf complexity by miRNA-regulated licensing of protein complexes. *Curr. Biol.* **24**, 2714-2719. doi:10.1016/j.cub.2014.09.058

Ryu, K. H., Huang, L., Kang, H. M. and Schiefelbein, J. (2019). Single-cell RNA sequencing resolves molecular relationships among individual plant cells. *Plant Physiol.* **179**, 1444-1456. doi:10.1104/pp.18.01482

Sablowski, R. (2016). Coordination of plant cell growth and division: collective control or mutual agreement? *Curr. Opin. Plant Biol.* **34**, 54-60. doi:10.1016/j.pbi.2016.09.004

Takada, S., Hibara, K., Ishida, T. and Tasaka, M. (2001). The CUP-SHAPED COTYLEDON1 gene of Arabidopsis regulates shoot apical meristem formation. *Development* **128**, 1127-1135.

Vernoux, T., Kronenberger, J., Grandjean, O., Laufs, P. and Traas, J. (2000). PIN-FORMED 1 regulates cell fate at the periphery of the shoot apical meristem. *Development* **127**, 5157-5165.

Vlad, D., Kierzkowski, D., Rast, M. I., Vuolo, F., Dello Ioio, R., Galinha, C., Gan, X., Hajheidari, M., Hay, A., Smith, R. S. et al. (2014). Leaf shape evolution through duplication, regulatory diversification, and loss of a homeobox gene. *Science* **343**, 780-783. doi:10.1126/science.1248384

Vroemen, C. W., Mordhorst, A. P., Albrecht, C., Kwaaitaal, M. A. and de Vries, S. C. (2003). The CUP-SHAPED COTYLEDON3 gene is required for boundary and shoot meristem formation in Arabidopsis. *Plant Cell* **15**, 1563-1577. doi:10.1105/tpc.012203

Zhang, T.-Q., Xu, Z.-G., Shang, G.-D. and Wang, J.-W. (2019). A single-cell RNA sequencing profiles the developmental landscape of arabidopsis root. *Mol. Plant* **12**, 648-660. doi:10.1016/j.molp.2019.04.004